Superadiabatic Multiphoton Landau–Zener–Stückelberg–Majorana Effect in a Transmon Qudit

Pei-Yao Song(宋佩瑶)[1], Jin-Lei Wu(吴金雷)[1*], and Shi-Lei Su(苏石磊)[1,2*]

[1]*School of Physics, Key Laboratory of Materials Physics of Ministry of Education, and International Laboratory for Quantum Functional Materials of Henan, Zhengzhou University, Zhengzhou 450001, China*
[2]*Institute of Quantum Materials and Physics, Henan Academy of Science, Zhengzhou 450046, China*

(Received 23 November 2025; accepted manuscript online 3 March 2026)

The recently observed two-photon Landau–Zener–Stückelberg–Majorana (LZSM) effect in superconducting circuits [*Phys. Rev. Lett.* **134** 060602 (2025)] has provided a robust pathway for high-fidelity population transfer in qudit systems, but its adiabatic nature necessitates long operation times, which are vulnerable to decoherence. In this paper, we present a practical acceleration scheme based on a superadiabatic (SUAD) framework that overcomes these fundamental limitations. Our approach is tailored to a multiphoton LZSM process. By constructing modified pulse envelopes for the existing drive field without introducing auxiliary counterdiabatic controls, we achieve accelerated high-fidelity state transfer from the ground state to the target excited state. For the two-photon case, our protocol reduces the operation time by more than four times compared with the adiabatic reference, while maintaining a fidelity of 0.998. We further generalize this to the three-photon regime, demonstrating a speedup factor exceeding three. Our SUAD LZSM scheme exhibits superior resilience to decoherence, offering a ready-to-implement solution for the fast and reliable control of multilevel quantum hardware.

DOI: 10.1088/0256-307X/43/4/040601 CSTR: 32039.14.0256-307X.43.4.040601

1. Introduction. The pursuit of high-dimensional quantum information processing (qudit-based QIP) has intensified the demand for fast, high-fidelity, and robust control protocols in multilevel quantum systems.[1–4] Superconducting transmons with anharmonic energy ladders serve as a leading platform for encoding and manipulating qudit states.[5–11] A pivotal advance in this context is the experimental demonstration of the two-photon Landau–Zener–Stückelberg–Majorana (LZSM) effect,[12] which enables coherent population transfer between nonadjacent levels (e.g., $|g\rangle \leftrightarrow |f\rangle$) via virtual intermediate states. This protocol leverages the inherent robustness of the adiabatic LZSM effect, making it resilient to certain control imperfections, which is a highly desirable feature for scalable quantum technologies.[13–18]

However, the adiabatic requirement of the conventional LZSM protocol imposes a substantial operational bottleneck, and the need for slow sweeps to suppress nonadiabatic transitions results in long control durations that are comparable to or even exceed the coherence times of the current devices.[19–23] This limitation is particularly acute for multiphoton processes, where the effective LZSM velocity scales with the photon number N. However, the required adiabatic condition can still lead to prohibitively slow operations for high-fidelity quantum state transfers. To address this challenge, shortcuts to adiabaticity (STA) have emerged as powerful tools to accelerate quantum dynamics.[24–31] Although various STA techniques exist, their direct application to multiphoton LZSM scenarios is nontrivial. Such a direct application features a complex interplay of couplings through multiple virtual intermediate states, leading to specific scaling relations for effective Rabi frequency and detuning.[32,33] Moreover, several STA protocols, such as those based on counterdiabatic (CD) driving, imposed directly on the transition between the initial and target states,[34–37] require the implementation of additional, often complex, control fields that can be experimentally demanding and introduce new sources of error.

In this study, we bridged this gap by developing a specialized superadiabatic (SUAD) protocol explicitly designed for the multiphoton LZSM effect. Building on the theoretical framework of second-order adiabatic states,[38–43] our key goal was to construct a modified driving Hamiltonian whose instantaneous eigenstates are the SUAD states of the original system. Critically, the modified Hamiltonian retains the same functional form as the reference LZSM Hamiltonian. It only requires modified time-dependent envelopes for the amplitude and the detuning of the original single-microwave drive. This is in stark contrast to the CD-based approaches, which require additional control lines or frequencies. We numerically demonstrated our SUAD–LZSM scheme for both two- and three-photon transitions in a transmon qudit. Our numerical simulations, based on the full multilevel Hamiltonian, show that the protocol achieves near-unity fidelity in a fraction of the duration required by the adiabatic method, while simultaneously exhibiting enhanced robustness against qudit

*Corresponding authors. Email: jlwu517@zzu.edu.cn; slsu@zzu.edu.cn
© 2026 Chinese Physical Society and IOP Publishing Ltd. All rights, including for text and data mining, AI training, and similar technologies, are reserved.

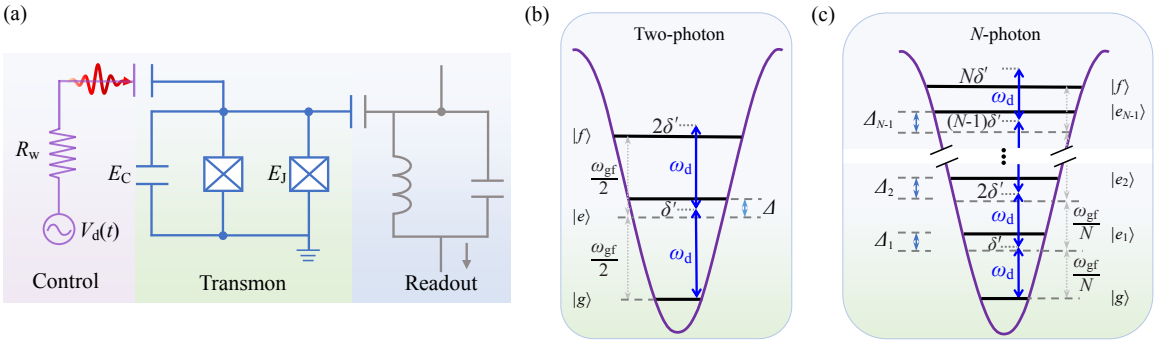

Fig. 1. Schematic of the multiphoton LZSM process in a superconducting transmon qudit system. (a) Circuit diagram of the capacitive coupling of a microwave drive line R_w [characterized by a time-dependent voltage $V_d(t)$] to a transmon superconducting qudit, connecting to the readout resonator. E_C is the charging energy, and E_J is the Josephson energy. (b) Schematic of the two-photon LZSM effect. The ground state $|g\rangle$ of a qutrit is excited to the second excited state $|f\rangle$ via the first excited state $|e\rangle$, with the time-dependent modulation $\omega_d(t)$ and a detuning Δ. (c) Schematic of the multiphoton LZSM effect for a qudit through $(N-1)$ intermediate excited states with the time-dependent modulation $\omega_d(t)$ and different detunings.

decay and dephasing. By providing a scalable, experimentally feasible, and minimally invasive acceleration strategy that directly builds upon the recent breakthroughs in Ref. [12], our study paves the way for practical high-speed qudit manipulation in superconducting quantum processors.

2. Model and Two-photon Effective Dynamics. As shown in Fig. 1, the system consists of a typical superconducting transmon circuit, including a transmon qubit with Josephson junctions, which can be measured using a readout resonator. The frequency is modulated by the magnetic flux using a local control line. We begin by focusing on a three-level system, as shown in Fig. 1(b), to illustrate the energy-level structure relevant to the two-photon LZSM process. The drive field with time-dependent frequency ω_d couples $|g\rangle$ to $|f\rangle$ via a virtual $|e\rangle$ excitation with the detuning Δ, which was experimentally confirmed by Ref. [12]. The transition frequencies were $\omega_{ge} = 2\pi \times 7.24\,\text{GHz}$ and $\omega_{ef} = 2\pi \times 6.90\,\text{GHz}$. Recalling the construction of a two-photon process in Ref. [12], in a rotation frame with the drive and after applying the rotating wave approximation, the Hamiltonian can be written as (assume $\hbar = 1$)

$$\begin{aligned}\hat{H}_{2p} = &-\Delta_{ge}|g\rangle\langle g| + \frac{\Omega_{ge}}{2}\left(|g\rangle\langle e| + |e\rangle\langle g|\right)\\ &+ \frac{\Omega_{ef}}{2}\left(|e\rangle\langle f| + |f\rangle\langle e|\right) + \Delta_{ef}|f\rangle\langle f|. \end{aligned} \tag{1}$$

For simplicity, we denote the Rabi frequency $\Omega_{ge} = \Omega$, whereas Ω_{ef} is scaled according to the ratio of the effective electric dipole moments of the two transitions $\Omega_{ef} = \sqrt{2}\Omega$.[44] The detunings of the drive from the respective transitions are given by $\Delta_{ge} = \omega_{ge} - \omega_d(t) - [\mathrm{d}\omega_d(t)/\mathrm{d}t]t$ and $\Delta_{ef} = \omega_{ef} - \omega_d(t) - [\mathrm{d}\omega_d(t)/\mathrm{d}t]t$. In the adiabatic LZSM scheme,[12] the drive frequency is a single-chirped microwave tone $\omega_d(t) = \omega_{gf}/2 - vt/2$. Moreover, the system is driven over the interval $t \in [-T/2, T/2]$, which results in a linear chirp rate $\mathrm{d}\omega_d(t)/\mathrm{d}t = -v/2$. The chirp amplitude is then determined by the LZSM velocity v and pulse duration T, yielding a modulation depth $D = \omega_d(T/2) - \omega_d(-T/2) = -vT/2$. In this case, $-\Delta_{ge}(t) = -\Delta - vt + \delta$ and $\Delta_{ef}(t) = -\Delta + vt - \delta$ are imposed.

The detuning $\Delta = \omega_{ge} - \omega_{gf}/2 = \omega_{gf}/2 - \omega_{ef} \approx E_C/2$ is determined by the anharmonicity of the transmon, where $E_C = 2\pi \times 318\,\text{MHz}$ is the charging energy, and the Josephson energy of $E_J \approx 2\pi \times 23\,\text{GHz}$. Following Ref. [12] to adiabatically transfer the population from $|g\rangle$ to $|f\rangle$ along one of the instantaneous eigenstates of the Hamiltonian in Eq. (1), the time-dependent super-Gaussian pulses $\Omega(t) = \Omega_0 \exp[K_c(2t/T)^n]$ are adopted, where K_c is the cutoff value, and n is the order of the super-Gaussian. We set $K_c = \ln(0.01)$ and $n = 4$. Based on second-order perturbation theory,[33] an effective low-frequency Hamiltonian can be derived in an adiabatic LZSM structure:

$$\hat{H}_{\text{eff}}^{(2\text{ph})} = -\frac{1}{2}(2vt - 2\delta)\hat{\sigma}_{gf}^{z} + \frac{\Omega_{gf}}{2}\hat{\sigma}_{gf}^{x}, \tag{2}$$

where $\hat{\sigma}_{gf}^{z} = |g\rangle\langle g| - |f\rangle\langle f|$ and $\hat{\sigma}_{gf}^{x} = |g\rangle\langle f| + |f\rangle\langle g|$ are Pauli matrices in the $\{|g\rangle, |f\rangle\}$ basis and $\Omega_{gf} = -\Omega_{ge}\Omega_{ef}/2\Delta$.

To construct a shortcut to the adiabatic LZSM process, we implemented a two-photon state transfer from $|g\rangle$ to $|f\rangle$ in an SUAD framework.[38–42] To this end, we considered the adiabatic states of the system, that is, the eigenstates in Eq. (2)

$$\begin{aligned}|\phi_+(t)\rangle &= \sin\frac{\theta(t)}{2}|f\rangle + \cos\frac{\theta(t)}{2}|g\rangle,\\ |\phi_-(t)\rangle &= \cos\frac{\theta(t)}{2}|f\rangle - \sin\frac{\theta(t)}{2}|g\rangle,\end{aligned} \tag{3}$$

corresponding to the energies

$$E_\pm(t) = \mathcal{C}(t) \equiv \sqrt{\Omega_{gf}^2/4 + (vt)^2},$$

for which the mixed angle is defined as $\theta(t) = \arccos[vt/C(t)]$, where $\delta = 0$. It is convenient to transform Eq. (2) to the presentation of adiabatic states with t-independent basis $\{|\phi_\pm\rangle\}$:

$$\begin{aligned}\hat{H}_1 &= \hat{U}^\dagger(t)\hat{H}_{\text{eff}}^{(2\text{ph})}\hat{U}(t) - \mathrm{i}\hat{U}^\dagger(t)\frac{\partial\hat{U}(t)}{\partial t}\\ &= \mathcal{C}(t)\sum_{l=\pm} l|\phi_l\rangle\langle\phi_l| + \frac{\mathrm{i}}{2}\frac{\partial\theta(t)}{\partial t}\left(|\phi_+\rangle\langle\phi_-| - |\phi_-\rangle\langle\phi_+|\right),\end{aligned} \tag{4}$$

where the unitary operator is $\hat{U}(t) = \sum_{l=\pm} |\phi_l(t)\rangle\langle\phi_l|$. From Eq. (4), when the adiabatic condition, $|\frac{\langle\phi_+|\dot{\hat{H}}_1|\phi_-\rangle}{E_+(t)-E_-(t)}| \ll 1$, i.e., $|2\mathcal{C}(t)| \gg |\frac{\partial_t\theta(t)}{2}|$, is satisfied well, the second term denoting the transitions between two adiabatic states can be omitted, which demands that $\theta(t)$ should be varied as slowly as possible. The second term of Eq. (4) $\hat{H}_{\rm ne} = \mathrm{i}\partial_t\theta(t)(|\phi_+\rangle\langle\phi_-| - |\phi_-\rangle\langle\phi_+|)/2$ affects the adiabatic evolution, termed "nonadiabatic error", which can be compensated to construct a shortcut to adiabatic passage for accelerating evolution by adding a CD term in the reduced Hamiltonian $\hat{H}_{\rm eff}^{(2\,\rm ph)}$ [24]

$$\hat{H}_{\rm CD} = -\hat{U}(t)\hat{H}_{\rm ne}\hat{U}^\dagger(t) = \frac{\mathrm{i}}{2}\frac{\partial\theta(t)}{\partial t}(|f\rangle\langle g| - |g\rangle\langle f|). \quad (5)$$

In this scenario, the reduced Hamiltonian $\hat{H}_{\rm eff}^{(2\rm ph)}$ can be modified as follows:

$$\hat{H}_m = \frac{\Omega_{\rm gf}}{2}\hat{\sigma}_x - \frac{1}{2}\frac{\partial\theta(t)}{\partial t}\hat{\sigma}_y - vt\hat{\sigma}_z. \quad (6)$$

However, this Hamiltonian significantly deviates from the two-photon adiabatic LZSM Hamiltonian in Eq. (2) because of the addition of a term involving $\hat{\sigma}_y$. This is similar to the implementation reported in Ref. [34], which is less robust than the two-photon LZSM process because of its sensitivity to errors in critical parameters, such as the phase, amplitude, and timing (see the Supplemental Material for Ref. [12]).

To proceed, we draw inspiration from the second-order adiabatic states, termed "SUAD states".[42] The SUAD states of the reduced system Hamiltonian are obtained from the eigenstates of $\hat{H}_1$ in Eq. (4) and can be expressed as

$$\begin{aligned}|\Phi_+(t)\rangle &= \mathrm{i}\cos\frac{\Theta(t)}{2}|\phi_+\rangle + \sin\frac{\Theta(t)}{2}|\phi_-\rangle,\\ |\Phi_-(t)\rangle &= \sin\frac{\Theta(t)}{2}|\phi_+\rangle + \mathrm{i}\cos\frac{\Theta(t)}{2}|\phi_-\rangle,\end{aligned} \quad (7)$$

corresponding to energies

$$E'_\pm(t) = \pm\mathcal{C}'(t) \equiv \pm\sqrt{\mathcal{C}(t)^2 + \dot{\theta}(t)^2/4},$$

where the supermixed angle is defined as $\Theta(t) = \arcsin\big[\partial_t\dot{\theta}(t)/2\mathcal{C}'(t)\big]$. In the frame defined by the t-independent SUAD states, the reduced Hamiltonian becomes

$$\begin{aligned}\hat{H}_2 &= \hat{\chi}^\dagger(t)\hat{H}_1\hat{\chi}(t) - \mathrm{i}\hat{\chi}^\dagger(t)\frac{\partial\hat{\chi}(t)}{\partial t}\\ &= \mathcal{C}'(t)\sum_{l=\pm} l|\Phi_l\rangle\langle\Phi_l|\\ &\quad - \frac{1}{2}\frac{\partial\Theta(t)}{\partial t}\big(|\Phi_+\rangle\langle\Phi_-| + |\Phi_-\rangle\langle\Phi_+|\big),\end{aligned} \quad (8)$$

with the SUAD transformation operator

$$\hat{\chi}(t) = \sum_{l=\pm}|\Phi_l(t)\rangle\langle\Phi_l|.$$

In this new frame, the nonadiabatic error,

$$\hat{H}'_{\rm ne} = -\partial_t\Theta(t)\big(|\Phi_+\rangle\langle\Phi_-| + |\Phi_-\rangle\langle\Phi_+|\big)/2,$$

can be offset by adding an SUAD CD term in the reduced Hamiltonian $\hat{H}'$:

$$\begin{aligned}\hat{H}'_{\rm CD} &= -\hat{U}(t)\hat{\chi}^\dagger(t)\hat{H}'_{\rm ne}\hat{\chi}(t)\hat{U}^\dagger(t)\\ &= \frac{\sin\theta(t)}{2}\frac{\partial_t\Theta(t)}{2}(|f\rangle\langle f| - |g\rangle\langle g|)\\ &\quad + \frac{\cos\theta(t)}{2}\frac{\partial_t\Theta(t)}{2}(|f\rangle\langle g| + |g\rangle\langle f|).\end{aligned} \quad (9)$$

By adding this CD term, a shortcut to the two-photon adiabatic LZSM process was constructed by modifying the reduced Hamiltonian $\hat{H}'$ to an SUAD version:

$$\hat{H}_{\rm s} = \frac{\Omega'_{\rm gf}}{2}(t)\hat{\sigma}_x - \delta'(t)\hat{\sigma}_z. \quad (10)$$

The modified coupling strength and detuning are as follows:

$$\begin{aligned}\Omega'_{\rm gf}(t) &= 2\mathcal{C}(t)\sin\theta(t) + \cos\theta(t)\frac{\partial\Theta(t)}{\partial t},\\ \delta'(t) &= \mathcal{C}(t)\cos\theta(t) - \frac{\sin\theta(t)}{2}\frac{\partial\Theta(t)}{\partial t}.\end{aligned} \quad (11)$$

Note that, here, we eliminate the Stark shifts of the energy levels as $(3\Omega'^2_{\rm ge} - 3\Omega'^2_{\rm ef} + \Omega'^2_{\rm fh})\sigma^z_{\rm gf}/12\Delta$ when we consider the involvement of the anharmonicity, that is, a leakage state $|h\rangle$ beyond the calculation subspace.[12] $\Omega'_{\rm ge}$, $\Omega'_{\rm ef}$, and $\Omega'_{\rm fh}$ are the modified superadiabatic pulses in generalized Eq. (1) as follows:

$$\begin{aligned}\hat{H}'_{\rm 2p} &= -\Delta_{\rm ge}|g\rangle\langle g| + \Delta_{\rm ef}|f\rangle\langle f| + \Delta_{\rm eh}|h\rangle\langle h|\\ &\quad + \frac{\Omega_{\rm ge}}{2}\big(|g\rangle\langle e| + |e\rangle\langle g|\big) + \frac{\Omega_{\rm ef}}{2}\big(|e\rangle\langle f| + |f\rangle\langle e|\big)\\ &\quad + \frac{\Omega_{\rm fh}}{2}\big(|f\rangle\langle h| + |h\rangle\langle f|\big),\end{aligned} \quad (12)$$

satisfying $\Omega'_{\rm ge} = (\sqrt{2}\Omega'_{\rm gf}\Delta)^{1/2}$ and $\Omega'_{\rm ge} = \Omega'_{\rm ef}/\sqrt{2} = \Omega'_{\rm fh}/\sqrt{3}$. This allowed us to proceed without additional compensation for the AC Stark shifts owing to the anharmonicity of the transmon qudit.

Note that $\hat{H}_{\rm s}$ instead of $\hat{H}_m$ in Eq. (6) does not introduce any additional terms to the reference two-photon LZSM Hamiltonian in Eq. (2), and both the coupling strength and detuning in the SUAD Hamiltonian are real. The reduced SUAD Hamiltonian is diagonal in the representation of the SUAD states. Therefore, the transmon system can evolve rapidly along the SUAD states without being limited by adiabatic conditions with a transient state.

$$|\psi(t)\rangle = \sum_{l=\pm}\eta'_l\exp\Big[-\mathrm{i}\int_0^z E'_l(t')\,\mathrm{d}t'\Big]|\Phi_l(t)\rangle, \quad (13)$$

where we ignore the geometric phases that are always zero during evolution. To implement the SUAD–LZSM scheme, for the transition from $|g\rangle$ to $|f\rangle$, the parameters can be varied, for example, from $\Theta(0) = 0$ and $\theta(0) = \pi$ to $\Theta(t_{\rm f}) = \theta(t_{\rm f}) = 0$.

For feasible experimentation, we used the single-photon LZSM velocity $v/2\pi = 62.5\,\mathrm{MHz/\mu s}$ in the following simulations of the two-photon case. The other parameters are $\Omega/2\pi = 55.6\,\mathrm{MHz}$ in the reference adiabatic LZSM scheme[12] and $\Omega/2\pi = 18.6\,\mathrm{MHz}$ in the SUAD–LZSM scheme ($\delta = 0$ in both schemes). We define the fidelity of implementing population transfer to

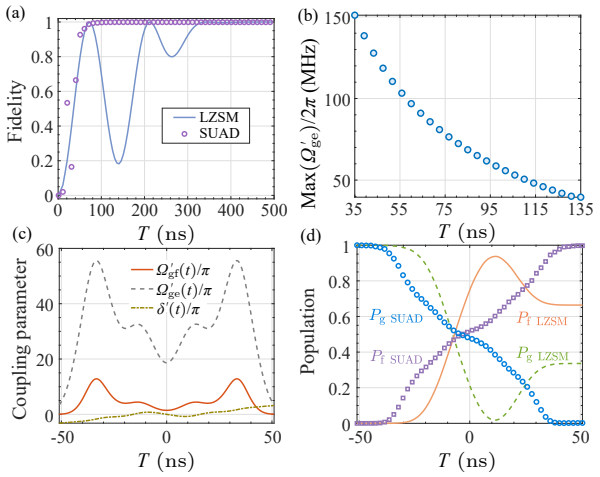

Fig. 2. Dynamics of two-photon processes. (a) Population of state $|f\rangle$ versus the total control duration T, comparing the adiabatic LZSM (blue solid line) and the proposed SUAD scheme (purple circles) for the $|g\rangle \to |f\rangle$ transfer fidelity. (b) Modified peak drive amplitude of $\Omega'_{\rm ge}/2\pi$ (MHz) for the SUAD scheme as a function of the control duration T. (c) Envelope of the modified Rabi frequency $\Omega'_{\rm ge}(t)$ (gray dashed line), effective $\Omega'_{\rm gf}(t)$ (red solid line), and detuning $\delta'(t)$ (yellow dotted line) with $T_m^{\rm 2p} = 102\,{\rm ns}$. (d) Population dynamics of the ground state $|g\rangle$ and the second excited state $|f\rangle$ under the two schemes with $T_m^{\rm 2p} = 102\,{\rm ns}$. The SUAD scheme (blue squares for $P_{\rm g}$, purple circles for $P_{\rm f}$) yields a monotonic, high-fidelity transfer from $|g\rangle$ to $|f\rangle$. The adiabatic LZSM (green dashed line for $P_{\rm g}$, orange solid line for $P_{\rm f}$) exhibits pronounced oscillations and residual ground-state population at the end of evolution.

$|f\rangle$ as $F = |\langle f|\psi_t\rangle|^2$, where $|\psi_t\rangle$ denotes the instantaneous state at time t calculated by numerically solving the Schrödinger equation with respect to the full Hamiltonian in Eq. (1). As shown in Fig. 2(a), we plot the population of state $|f\rangle$ over the control duration T for the two schemes governed by the modified full Hamiltonian Eq. (1) when the initial state is $|g\rangle$. The SUAD scheme converges to near unity (80 ns), which is four times faster than the adiabatic LZSM scheme (330 ns). Figure 2(b) shows the variation in the maximum value of $\Omega'_{\rm ge}$ modified in the SUAD scheme over the control duration, from which we know that only by setting $T = 102\,{\rm ns}$ can the maximum value of $\Omega'_{\rm ge}$ (corresponding to $\Omega/2\pi = 18.6\,{\rm MHz}$) be the same as the reference value $\max[\Omega_{\rm ge}(t)]/2\pi = 55.6\,{\rm MHz}$ in the adiabatic LZSM scheme.[12] Therefore, for fairness, we chose $T_m^{\rm 2p} = 102\,{\rm ns}$ with the maximum value $\Omega'_{\rm ge}/2\pi = 55.6\,{\rm MHz}$ during $[-T_m/2, T_m/2]$. Figure 2(c) shows the envelopes of the coupling strength and detuning in Eq. (11). Based on this duration setting, we compare the population transfers of the two schemes in Fig. 2(d). The SUAD–LZSM scheme steadily achieves a near-perfect quantum state transfer with evolution during $[-51, 51]\,{\rm ns}$, whereas a noticeable oscillation is observed at the end of the evolution in the reference LZSM scheme. Specifically, the state fidelity of $|f\rangle$ approaches 0.998, which is significantly higher than that of the reference LZSM scheme (less than 0.7).[12] In comparison to the SUAD control technology in the transmon system experimentally achieved in Ref. [34,45], their study introduced additional single-photon control CD terms between the states $|g\rangle$ and $|f\rangle$, whereas our scheme modified the time-domain envelope of the reference Hamiltonian, thus further reducing the experimental complexity.

3. Multiphoton Superadiabatic LZSM Effect. Owing to the observed doubling of the LZSM velocity in the two-photon LZSM effect,[12] it is natural to obtain an N-fold LZSM velocity by generalizing the two-photon LZSM effect to the N-photon situation. To implement the N-photon LZSM effect, an $(N+1)$-level structure should be considered, including the ground state $|g\rangle$, jth excited state $|e_j\rangle$ $(j = 1, 2, 3, \ldots, N-1)$, and Nth excited state $|f\rangle$, as shown in Fig. 1(c).

We consider the three-photon case to illustrate our SUAD version of the multiphoton LZSM effect. To this end, considering the three higher excited states $|e_1\rangle$, $|e_2\rangle$, and $|f\rangle$ in addition to the ground state $|g\rangle$, the drive field $\omega_{\rm d}(t)$ induces a three-photon transition through the intermediate levels $|e_1\rangle$ and $|e_2\rangle$ with different detunings Δ_1 and Δ_2, respectively. In the interaction picture, we can write the Hamiltonian, including the two intermediate states, as follows:

$$\begin{aligned}\hat{H}_{\rm 3p} = &\frac{\hbar\Omega_{\rm ge_1}}{2}{\rm e}^{-{\rm i}(\omega_{\rm ge_1}-\omega_{\rm d})t}|g\rangle\langle e_1| \\ &+ \frac{\hbar\Omega_{\rm e_1e_2}}{2}{\rm e}^{-{\rm i}(\omega_{\rm e_1e_2}-\omega_{\rm d})t}|e_1\rangle\langle e_2| \\ &+ \frac{\hbar\Omega_{\rm e_2f}}{2}{\rm e}^{-{\rm i}(\omega_{\rm e_2f}-\omega_{\rm d})t}|e_2\rangle\langle f| + {\rm H.c.} \end{aligned} \tag{14}$$

In the adiabatic reference framework, we define $\epsilon(t) = \omega_{\rm d}(t) - \omega_{\rm gf}/3 = Dt/T = -vt/2$, corresponding to the notation used for a two-photon process with $\Delta_1 = \omega_{\rm ge_1} - \omega_{\rm d}$ and $\Delta_2 = \omega_{\rm d} - \omega_{\rm e_2f}$. The experimental parameters for the transition frequencies are provided in Ref. [12]: $\omega_{\rm ge_1} = 2\pi \times 7.24\,{\rm GHz}$, $\omega_{\rm e_1e_2} = 2\pi \times 6.90\,{\rm GHz}$, and $\omega_{\rm e_2f} = 2\pi \times 6.53\,{\rm GHz}$. In this case, we set the single-photon LZSM velocity $v/2\pi = 0.19\,{\rm MHz/\mu s}$. The full Hamiltonian in Eq. (14) can be simplified to a third-order effective version[32]

$$\begin{aligned}\hat{H}_{\rm eff}^{(3)} = &\sum_{l,m,n}\Big\{\frac{1}{\omega_n(\omega_n-\omega_m)}[\hat{h}_l^\dagger\hat{h}_m\hat{h}_n^\dagger{\rm e}^{-{\rm i}(\omega_l-\omega_m+\omega_n)t} \\ &+ \hat{h}_l\hat{h}_m\hat{h}_n^\dagger{\rm e}^{{\rm i}(\omega_l+\omega_m-\omega_n)t} + \hat{h}_l\hat{h}_m^\dagger\hat{h}_n{\rm e}^{{\rm i}(\omega_l-\omega_m+\omega_n)t} \\ &+ \hat{h}_l^\dagger\hat{h}_m^\dagger\hat{h}_n{\rm e}^{-{\rm i}(\omega_l+\omega_m-\omega_n)t}] \\ &+ \frac{1}{\omega_n(\omega_n+\omega_m)}[\hat{h}_l^\dagger\hat{h}_m\hat{h}_n{\rm e}^{{\rm i}(\omega_m+\omega_n-\omega_l)t} \\ &+ \hat{h}_l\hat{h}_m^\dagger\hat{h}_n^\dagger{\rm e}^{{\rm i}(\omega_l-\omega_m-\omega_n)t}]\Big\}. \end{aligned} \tag{15}$$

Through a rotational transformation $U = \exp(-{\rm i}3\epsilon\hat{\sigma}_z^{\rm g}t/2)$, we obtain the final effective Hamiltonian

$$\hat{H}_{\rm LZSM}^{(\rm 3ph)} = -\frac{\hbar 3vt}{2}\hat{\sigma}_z^{\rm gf} - \frac{\hbar\Omega_{\rm gf}}{2}\hat{\sigma}_x^{\rm gf}, \tag{16}$$

for which we define the three-photon Rabi frequency $\Omega_{\rm gf} \equiv \sqrt{6}\Omega^3/4\Delta_1\Delta_2$ as $\Omega_{\rm ge_1} = \Omega_{\rm e_1e_2}/\sqrt{2} = \Omega_{\rm e_2f}/\sqrt{3} = \Omega$. This reveals an evident LZSM structure between the ground state $|g\rangle$ and the third excited state $|f\rangle$. Furthermore, for N-photon LZSM, we provide the general form:

$$\hat{H}_{\rm LZSM}^{(N\rm ph)} = -\frac{\hbar Nvt}{2}\hat{\sigma}_z^{\rm gf} - \frac{\hbar\Omega_{\rm gf}}{2}\hat{\sigma}_x^{\rm gf}, \tag{17}$$

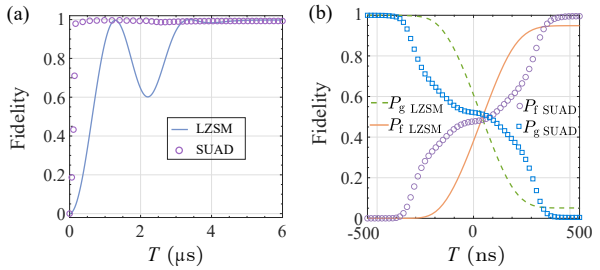

Fig. 3. Dynamics of three-photon processes. (a) Fidelity versus total control duration T, comparing the adiabatic LZSM (blue solid line) and the proposed SUAD scheme (purple circles) for the transition $|g\rangle \rightarrow |f\rangle$. (b) Population dynamics $P_{\rm g\ SUAD}$ (blue squares) of the ground state $|g\rangle$ for SUAD and $P_{\rm g\ LZSM}$ (green dashed) for the adiabatic scheme. Population $P_{\rm f\ SUAD}$ (purple circles) of the third excited state $|f\rangle$ for SUAD, and $P_{\rm g\ LZSM}$ (orange solid) for the adiabatic scheme at $T_m^{\rm 3p} = 1100\,$ns.

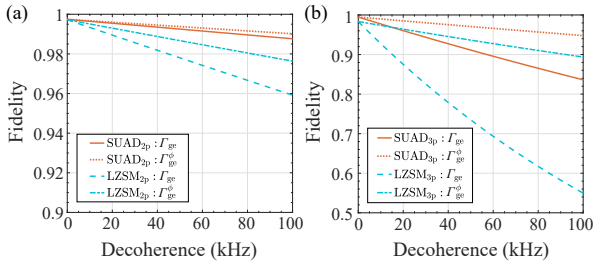

Fig. 4. Robustness of the (a) two- and (b) three-photon LZSM effects against decoherence, with the decay rate $\Gamma_{\rm ge}$ ($\Gamma_{\rm ge_1}$) and pure dephasing rate $\Gamma_{\rm ge}^{\phi}$ ($\Gamma_{\rm ge_1}^{\phi}$), respectively, varied from 0 to 100 kHz. The red line represents the SUAD scheme, and the cyan dashed line represents the previous LZSM.

where $\Omega_{\rm gf} \equiv \sqrt{N!}\Omega^N/2^{N-1}\prod_{k=1}^{N-1}\Delta_k$ corresponds to the N-photon Rabi frequency. In the case of the three-photon LZSM effect, the LZSM velocity becomes three times that of the single-photon case, and the N-photon process yields an N-times enhancement. Similar to the two-photon SUAD scheme, we can modify the effective three-photon Rabi frequency and detuning to implement the SUAD three-photon LZSM effect. We conduct relevant numerical simulations, as shown in Fig. 3. Figure 3(a) shows the population of state $|f\rangle$ over the control duration T for the two schemes governed by the modified full Hamiltonian Eq. (15). The fidelity of the three-photon SUAD scheme exceeds 0.996 at approximately 1 μs, whereas the adiabatic LZSM scheme requires more than 3.5 μs to ensure that the fidelity remains above 0.996. Therefore, the proposed SUAD scheme is more than three times faster than the adiabatic scheme. Subsequently, we selected the duration $T_m = 1.1\,\mu$s corresponding to the peak driving coupling strength of $\Omega_{\rm ge_1}/2\pi = 55.6\,$MHz applied in the experiment.[12] We then observed the population of the initial $|g\rangle$ and final $|f\rangle$ states in the two schemes in Fig. 3(b). The proposed SUAD scheme has an apparent advantage in terms of the final fidelity of the state $|f\rangle$. Note that the final fidelity near 0.95 in the adiabatic LZSM scheme contributes to the resonant nonadiabatic dynamics [the first peak of the blue line in Fig. 3(a)], which does not tolerate deviations in the system control parameters.

4. Robustness to Decoherence. In previous sections, we focused on the dynamic process and ignored the effects of system decoherence during evolution. Here, we consider the decay and dephasing in the evolution of the transmon system using the Lindblad master equation[46,47]

$$\begin{aligned}\dot{\rho}_{\rm 2p} &= {\rm i}[\rho, \hat{H}_{\rm 2p}] + \frac{\Gamma_{\rm 2p}}{2}\hat{\mathcal{L}}(\hat{\sigma}_{\rm 2p}) + \frac{\Gamma_{\rm 2p}^{\phi}}{2}\hat{\mathcal{L}}(\hat{\sigma}_{\rm 2p}^{\phi}),\\ \dot{\rho}_{\rm 3p} &= {\rm i}[\rho, \hat{H}_{\rm 3p}] + \frac{\Gamma_{\rm 3p}}{2}\hat{\mathcal{L}}(\hat{\sigma}_{\rm 3p}) + \frac{\Gamma_{\rm 3p}^{\phi}}{2}\hat{\mathcal{L}}(\hat{\sigma}_{\rm 3p}^{\phi}),\end{aligned} \tag{18}$$

where ρ is the density matrix of the transmon system. $\hat{\mathcal{L}}(\hat{\mathcal{A}}_j) = 2\hat{\mathcal{A}}_j\rho\hat{\mathcal{A}}_j^{+} - \hat{\mathcal{A}}_j^{+}\hat{\mathcal{A}}_j\rho - \rho\hat{\mathcal{A}}_j^{+}\hat{\mathcal{A}}_j$ is the Lindbladian operator for the operator $\hat{\mathcal{A}}$. $\hat{\sigma}_{\rm 2p} = (|g\rangle\langle e|) + \sqrt{2}(|e\rangle\langle f|) + \sqrt{3}|f\rangle\langle h|$ and $\hat{\sigma}_{\rm 2p}^{\phi} = |e\rangle\langle e| + 2|f\rangle\langle f| + 3|h\rangle\langle h|$ represent decay and pure dephasing terms for the two-photon process, respectively. $\hat{\sigma}_{\rm 3p} = (|g\rangle\langle e_1|) + \sqrt{2}(|e_1\rangle\langle f|) + \sqrt{3}|e_2\rangle\langle f| + 2|f\rangle\langle h|$ and $\hat{\sigma}_{\rm 3p}^{\phi} = |e_1\rangle\langle e_1| + 2|e_2\rangle\langle e_2| + 3|f\rangle\langle f| + 4|h\rangle\langle h|$ are used for the three-photon case. $\Gamma_{\rm 2p} = \Gamma_{\rm ge}$ ($\Gamma_{\rm 2p}^{\phi} = \Gamma_{\rm ge}^{\phi}$) and $\Gamma_{\rm 3p} = \Gamma_{\rm ge_1}$ ($\Gamma_{\rm 3p}^{\phi} = \Gamma_{\rm ge_1}^{\phi}$) are the decay (dephasing) rates of the transmon qudit for the two- and three-photon cases, respectively. For the two schemes in the two- and three-photon cases, we chose their control durations converging to the corresponding relatively high fidelity, that is, $T_m^{\rm 2p} = 102\,$ns and $T_m^{\rm 3p} = 1.1\,\mu$s for the SUAD scheme, and $T_m^{\rm 2p} = 400\,$ns[12] and $T_m^{\rm 3p} = 4\,\mu$s for the adiabatic LZSM scheme, respectively. Subsequently, we separately considered the decay rate and pure dephasing rate varying within the range of 0–100 kHz, and the results are presented in Fig. 4. As the decoherence increases, the fidelity gradually decreases. However, the SUAD scheme demonstrates stronger robustness to the decay and dephasing of transmons. For a fair comparison, we considered the decay rate implemented in Ref. [12]: $\Gamma_{\rm ge} = \Gamma_{\rm ge_1} = 33\,$kHz, and the dephasing rates $\Gamma_{\rm ge}^{\phi}$ and $\Gamma_{\rm ge_1}^{\phi}$ are set to the same values. The fidelity of the SUAD two-photon scheme can reach 0.995 (0.9965) when we consider the decay (dephasing), whereas that of the adiabatic scheme is approximately 0.98 (0.994), as shown in Fig. 4(a) and reported in Ref. [12]. The robustness of the three-photon SUAD LZSM scheme is more pronounced, with a fidelity of 0.938 (0.98) at 33 kHz when the decay (dephasing) is considered, whereas that of the adiabatic LZSM scheme decreases to approximately 0.8 (0.95), as in Fig. 4(b).

5. Conclusion. In summary, we proposed and analyzed an SUAD approach to accelerate multiphoton LZSM transitions in a superconducting transmon qudit system. By constructing modified SUAD Hamiltonians in both the two- and three-photon regimes, we effectively suppressed nonadiabatic transitions and enabled fast high-fidelity population transfer from the ground state $|g\rangle$ to the target excited state $|f\rangle$. Our numerical simulations demonstrate that the SUAD–LZSM scheme achieves near-unity fidelity in approximately one-fourth of the time required by adiabatic LZSM methods while also exhibiting superior robustness against the decay and dephasing of the transmon. The modified microwave pulse shapes and detunings derived from SUAD formalism are experimentally feasible and compatible with existing superconducting circuit control techniques. These results establish the

SUAD–LZSM framework as a powerful tool for robust and efficient quantum-state manipulation in multilevel systems with potential applications in QIP and state preparation. Future studies can extend this approach to higher-order multiphoton processes or other physical platforms beyond superconducting circuits.

Acknowledgments. This work was supported by the National Natural Science Foundation of China (Grant Nos. 12575032, 62571494, 12304407, and 12274376), the Natural Science Foundation of Henan Province (Grant No. 232300421075), and the China Postdoctoral Science Foundation (Grant Nos. 2023TQ0310 and 2024M762973).

References

[1] Luo K, Huang W, Tao Z, Zhang L, Zhou Y, Chu J, Liu W, Wang B, Cui J, Liu S, Yan F, Yung M H, Chen Y, Yan T, and Yu D 2023 *Phys. Rev. Lett.* **130** 030603
[2] Zhou H, Gao H, Leitao N T, Makarova O, Cong I, Douglas A M, Martin L S, and Lukin M D 2024 *Phys. Rev. X* **14** 031017
[3] Tripathi V, Goss N, Vezvaee A, Nguyen L B, Siddiqi I, and Lidar D A 2025 *Phys. Rev. Lett.* **134** 050601
[4] Meng Z, Liu W Q, Song B W, Wang X Y, Zhang A N, and Yin Z Q 2024 *Phys. Rev. A* **109** 022612
[5] Li S, Zhu Y K, Zhang W X, Pan D J, Liao W C, Lv Q X, Yu H F, Yu Y, Xue Z Y, Yan H, and Zhu S L 2025 *Phys. Rev. Lett.* **135** 200802
[6] Zhang J, Huang W, Chu J, Qiu J, Sun X, Tao Z, Zhang J, Zhang L, Zhou Y, Chen Y, Liu Y, Liu S, Zhong Y, Miao J J, Niu J, and Yu D 2025 *Phys. Rev. Lett.* **134** 070601
[7] Kehrer T, Nadolny T, and Bruder C 2024 *Phys. Rev. Res.* **6** 013050
[8] Wu Z H, Lei L X, Zhang X F, Xue S C, Hu S, Li C, Fu X, Chen P X, Lu K, Deng M T, and Wu J J 2025 *Chin. Phys. Lett.* **42** 040501
[9] Yun M R, Shan Z, Sun L L, Yan L L, Jia Y, Su S L, and Chen G 2024 *Phys. Rev. A* **110** 022608
[10] Tripathi V, Chen H, Khezri M, Yip K W, Levenson-Falk E, and Lidar D A 2022 *Phys. Rev. Appl.* **18** 024068
[11] Kervinen M, Ramírez-Muñoz J, Välimaa A, and Sillanpää M 2019 *Phys. Rev. Lett.* **123** 240401
[12] Björkman I, Kuzmanović M, and Paraoanu G S 2025 *Phys. Rev. Lett.* **134** 060602
[13] Ryzhov A I, Ivakhnenko O V, Shevchenko S N, Gonzalez-Zalba M F, and Nori F 2024 *Phys. Rev. Res.* **6** 033340
[14] Poletto S, Gambetta J M, Merkel S T, Smolin J A, Chow J M, Córcoles A D, Keefe G A, Rothwell M B, Rozen J R, Abraham D W, Rigetti C, and Steffen M 2012 *Phys. Rev. Lett.* **109** 240505
[15] Morvan A, Ramasesh V V, Blok M S, Kreikebaum J M, O'Brien K, Chen L, Mitchell B K, Naik R K, Santiago D I, and Siddiqi I 2021 *Phys. Rev. Lett.* **126** 210504
[16] Blok M S, Ramasesh V V, Schuster T, O'Brien K, Kreikebaum J M, Dahlen D, Morvan A, Yoshida B, Yao N Y, and Siddiqi I 2021 *Phys. Rev. X* **11** 021010
[17] Cervera-Lierta A, Krenn M, Aspuru-Guzik A, and Galda A 2022 *Phys. Rev. Appl.* **17** 024062
[18] Zhang H, Chakram S, Roy T, Earnest N, Lu Y, Huang Z, Weiss D K, Koch J, and Schuster D I 2021 *Phys. Rev. X* **11** 011010
[19] Albash T and Lidar D A 2018 *Rev. Mod. Phys.* **90** 015002
[20] Xu J, Zhang Y, Zheng W, Cai H, Zhou H, Li X, Liao X, Zhang Y, Li S, Lan D, Tan X, and Yu Y 2024 *Chin. Phys. Lett.* **41** 040202
[21] Tan X S, Zhang D W, Zhang Z T, Yu Y, Han S Y, and Zhu S L 2014 *Phys. Rev. Lett.* **112** 027001
[22] Johansson J, Amin M H S, Berkley A J, Bunyk P, Choi V, Harris R, Johnson M W, Lanting T M, Lloyd S, and Rose G 2009 *Phys. Rev. B* **80** 012507
[23] Kuzmanović M, Björkman I, McCord J J, Dogra S, and Paraoanu G S 2024 *Phys. Rev. Res.* **6** 013188
[24] Guéry-Odelin D, Ruschhaupt A, Kiely A, Torrontegui E, Martínez-Garaot S, and Muga J G 2019 *Rev. Mod. Phys.* **91** 045001
[25] An S, Lv D, del Campo A, and Kim K 2016 *Nat. Commun.* **7** 12999
[26] Yin Z, Li C, Allcock J, Zheng Y, Gu X, Dai M, Zhang S, and An S 2022 *Nat. Commun.* **13** 188
[27] Song W, Liu X, Sun J, You O, Wu S, Chen C, Zhu S, Li T, and Zhang S 2025 *Sci. Adv.* **11** eadt7224
[28] Chen X, Torrontegui E, and Muga J G 2011 *Phys. Rev. A* **83** 062116
[29] Li M M, Tan X S, Dai K Z, Zhao P, Yu H F, and Yu Y 2018 *Chin. Phys. B* **27** 063202
[30] Zhu X Y, Zhu L T, Guo G C, Tu T, and Li C F 2025 *Phys. Rev. A* **111** 012621
[31] Chen Y H, Qin W, Wang X, Miranowicz A, and Nori F 2021 *Phys. Rev. Lett.* **126** 023602
[32] Shao W, Wu C, and Feng X L 2017 *Phys. Rev. A* **95** 032124
[33] James D F and Jerke J 2007 *Can. J. Phys.* **85** 625
[34] Vepsäläinen A, Danilin S, and Paraoanu G S 2019 *Sci. Adv.* **5** eaau5999
[35] Du Y X, Liang Z T, Li Y C, Yue X X, Lv Q X, Huang W, Chen X, Yan H, and Zhu S L 2016 *Nat. Commun.* **7** 12479
[36] Chen X, Lizuain I, Ruschhaupt A, Guéry-Odelin D, and Muga J G 2010 *Phys. Rev. Lett.* **105** 123003
[37] Chen Y H, Xia Y, Wu Q C, Huang B H, and Song J 2016 *Phys. Rev. A* **93** 052109
[38] Berry M V 1987 *Proc. R. Soc. Lond. A* **414** 31
[39] Ibáñez S, Chen X, Torrontegui E, Muga J G, and Ruschhaupt A 2012 *Phys. Rev. Lett.* **109** 100403
[40] Baksic A, Ribeiro H, and Clerk A A 2016 *Phys. Rev. Lett.* **116** 230503
[41] Zhou B, Baksic A, Ribeiro H, Yale C, Heremans F, Jerger P, Auer A, Burkard G, Clerk A, and Awschalom D 2017 *Nat. Phys.* **13** 330
[42] Wu J L, Su S L, Ji X, and Zhang S 2017 *Ann. Phys.* **386** 34
[43] Torrontegui E, Ibáñez S, Martínez-Garaot S, Modugno M, del Campo A, Guéry-Odelin D, Ruschhaupt A, Chen X, and Muga J G 2013 *Adv. At. Mol. Opt. Phys.* **62** 117
[44] Koch J, Yu T M, Gambetta J, Houck A A, Schuster D I, Majer J, Blais A, Devoret M H, Girvin S M, and Schoelkopf R J 2007 *Phys. Rev. A* **76** 042319
[45] Vepsäläinen A, Danilin S, and Paraoanu G S 2018 *Quantum Sci. Technol.* **3** 024006
[46] Xu J, Li S, Chen T, and Xue Z Y 2020 *Front. Phys.* **15** 41503
[47] Liang Y, Wu, Y X, and Xue Z Y 2024 *Phys. Rev. Appl.* **22** 024061